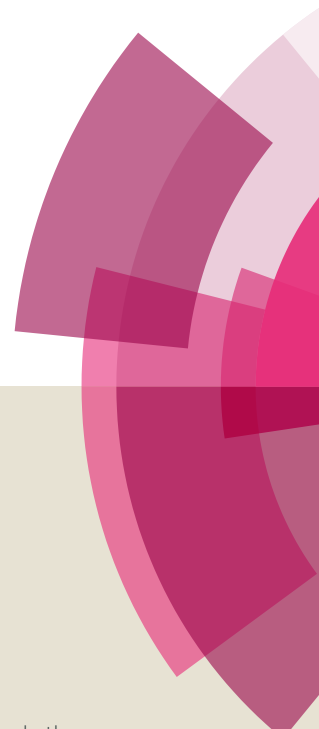
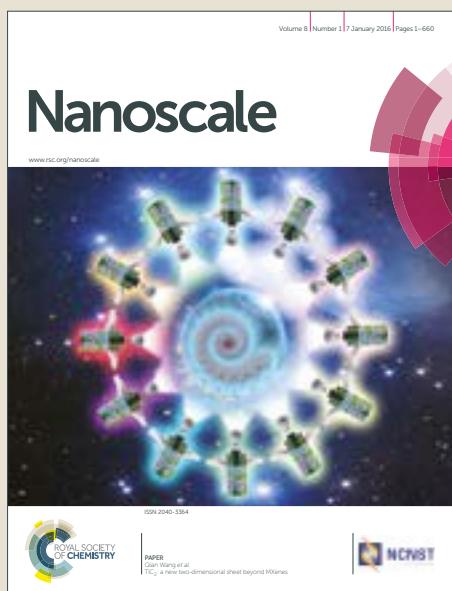


Nanoscale

Accepted Manuscript



This article can be cited before page numbers have been issued, to do this please use: D. Amgar, T. binyamin, V. Uvarov and L. Etgar, *Nanoscale*, 2018, DOI: 10.1039/C7NR09607K.



This is an Accepted Manuscript, which has been through the Royal Society of Chemistry peer review process and has been accepted for publication.

Accepted Manuscripts are published online shortly after acceptance, before technical editing, formatting and proof reading. Using this free service, authors can make their results available to the community, in citable form, before we publish the edited article. We will replace this Accepted Manuscript with the edited and formatted Advance Article as soon as it is available.

You can find more information about Accepted Manuscripts in the [author guidelines](#).

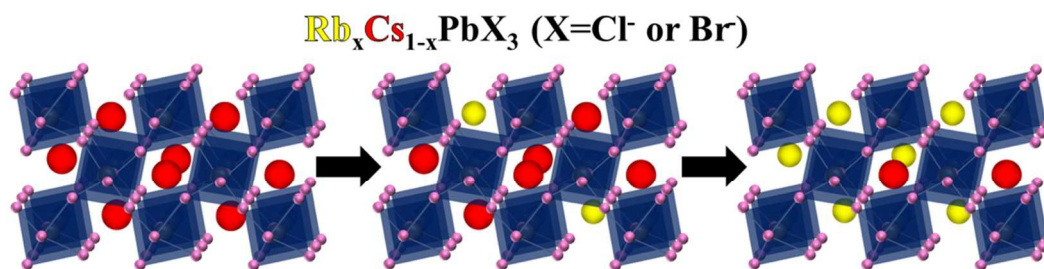
Please note that technical editing may introduce minor changes to the text and/or graphics, which may alter content. The journal's standard [Terms & Conditions](#) and the ethical guidelines, outlined in our [author and reviewer resource centre](#), still apply. In no event shall the Royal Society of Chemistry be held responsible for any errors or omissions in this Accepted Manuscript or any consequences arising from the use of any information it contains.

Near ultra-violet to mid-visible band gap tuning of mixed cation $\text{Rb}_x\text{Cs}_{1-x}\text{PbX}_3$ (X=Cl or Br) perovskite nanoparticles

Daniel Amgar, Tal Binyamin, Vladimir Uvarov, Lioz Etgar*

The Institute of Chemistry, The Center for Nanoscience and Nanotechnology, The Casali Center for Applied Chemistry, The Hebrew University of Jerusalem, Jerusalem, Israel

*E-mail: lioz.etgar@mail.huji.ac.il



TOC Graphic

Abstract

One of the most attractive features of perovskite materials is their chemical flexibility. Due to innovative chemical compositions of perovskite, the optical, structural, and functionalities became more advanced, enabling better solar performance in photovoltaics, as well as robustness and excellent properties in the nanoscale for optoelectronics. The quest for novel perovskite compositions in the nano-scale is significantly important. This paper reports on a mixed-cation system of $\text{Rb}_x\text{Cs}_{1-x}\text{PbX}_3$ (where X=Cl or Br) nanoparticles. The absorption of the nanoparticles is tunable in the near ultra-violet and visible regions between ~ 395 - 525 nm for $\text{Rb}_x\text{Cs}_{1-x}\text{PbX}_3$ ($x=0$ to $x=0.8$ and X=Cl or Br). The photoluminescence quantum yields (PLQY) of the mixed Rb^+/Cs^+ nanoparticle systems are comparable to the PLQY of CsPbX_3 nanoparticles. Interestingly the attempt to synthesize Cl- and Br-based nanoparticles with high Rb^+ content succeeded, although possessing low tolerance factors. We conclude that these mixed Rb^+/Cs^+ nanoparticles are more adjustable to structural distortions caused by the cation substitutions than their bulk counterparts, what opens a way towards developing more advanced mixed-ion perovskite compositions in the nano-scale.

Key words:

Mixed cation perovskite, inorganic perovskite nanoparticles, rubidium

Introduction

Lead halide perovskite materials are being studied intensively in the past years for their outstanding photovoltaic activity. The formula that defines the perovskite is AMX_3 and it enables high diversity, from organic-inorganic hybrids to all-inorganic perovskites, mostly known as methylammonium lead halide ($MAPbX_3$; $X=Cl, Br, I$) or cesium lead halide ($CsPbX_3$; $X=Cl, Br, I$) compositions. The diverse nature of perovskites encouraged investigation of advanced perovskite materials using chemical modifications. A lot of reports were focused on substitution of the monovalent cation [$A=$ methylammonium (MA) CH_3NH_3 , formamidinium (FA) $CH_3(NH_2)_2$, or Cs^+], divalent metal cation ($M= Pb^{2+}$, Sn^{2+} and Ge^{2+}), and the halide ($X= Cl^-, Br^-$ or I^-).¹⁻¹³ Chemical modifications for perovskites are of great importance, enabling band-gap engineering, adjustment of properties for specific requirements, refraining from toxic compounds, improvements of the synthetic routes, enhancing product quality, and so on. In the solar field, the most efficient perovskite-based solar cell was fabricated with a mixed-cation perovskite composition, reaching 22.1%, which emphasizes the importance of chemically modified perovskites.^{14,15} Apart from bulk perovskites, mixed-halide systems in the nano-scale were investigated thoroughly,^{16,17,18} while mixed-cation systems are still behind for both hybrid organic inorganic and all-inorganic perovskite nanoparticles (NPs). Recently, the mixed-cation system was applied for NPs by Protesescu et al. that reported on $FAPbI_3$ and $(FA/Cs)PbI_3$ perovskite NPs with improved robustness, relative to MA- or Cs-based perovskite NPs, and emissions in the near-infrared spectral regions.¹⁹ Moreover, Liu et al. proposed a mixed-metal cation system of $CsPb_xMn_{1-x}Cl_3$ and revealed a new perspective for tuning the optical properties of perovskite NPs.⁹

The optical properties of perovskite NPs are mainly affected by the electronic structure, while structural distortions are known to influence as well. By considering the specific geometry required for an ideal perovskite, only specific combination of ions will be suitable. The Goldschmidt tolerance factor (TF) aimed to predict a stable perovskite

structure, relating to a 3D-cubic close packing of ions.^{20,21,22} For ideal cubic structure the TF is calculated as follows; $t = (r_A + r_X)/\sqrt{2}(r_M + r_X)$, where r is the ionic radius, and the empirical formability range is $0.8 < t < 1.0$.²³ Considering the TF restrictions, most of the monovalent elemental cations are mismatched to establish a stable perovskite. Recently, rubidium cation (Rb^+) was suggested to balance the TF for a better solar efficiency and better perovskite stability due to its non-oxidative nature.¹² Another work by Linaburg et al. describes solid solutions of inorganic mixed-cation $\text{Cs}_{1-x}\text{Rb}_x\text{PbX}_3$ ($\text{X}=\text{Cl}$ or Br) perovskites showing the adjustable manner of perovskites, and exploring their structural and optical response to changes in the TF. This gave a new insight about the lower limit of the TF in which perovskite remains stable at room temperature.¹³ Nonetheless mixed-cation systems were studied in the bulk form, mixed-cation perovskites in the nano-scale remain poorly explored. In general, small perovskite NPs are known to adjust their strain distribution and lattice parameters, compared with the bulk form. Therefore, the structural flexibility of perovskite NPs to A-cation substitutions, full or partial, is assumed to be different in the nano-scale due to a more adjustable nature of contraction and expansion of the structure.^{19,24} RbPbCl_3 and RbPbBr_3 compositions are yet to be successfully synthesized due to the small Rb^+ cation, and relatively small TF values of 0.806 and 0.801, respectively; Motivated by the structural suppleness and the option to achieve higher TFs by mixing different cations, we successfully synthesized Rb^+/Cs^+ -based lead halide perovskite NPs with the tunable composition of $\text{Rb}_x\text{Cs}_{1-x}\text{PbX}_3$ ($x=0, 0.2, 0.6, 0.8$; $\text{X}=\text{Cl}, \text{Br}$). Characterizations revealed new insights regarding the crystal structure and the degree of flexibility of the octahedral PbX_6 network while the optical properties were tuned based on the Rb^+/Cs^+ ratio. The NPs exhibit photoluminescence quantum yields (PLQY) of up to $\sim 60\%$, tunable emissions in the visible, and intriguing structural changes upon increasing Rb^+ content in the crystal. The results show an approximated upper limit of $x=0.8$ for $\text{Rb}_x\text{Cs}_{1-x}\text{PbX}_3$ yielding absorption peaks, which are blue shifted compared with CsPbX_3 NPs. For the nominal $x=1$ Cl-based NPs, a structural change into $\text{Rb}_6\text{Pb}_5\text{Cl}_{16}$ phase was observed and explored in our recently published work.²⁵ In the case of $x=1$ for Br-based NPs, the NPs were failed to form. Energy dispersive x-ray spectroscopy (EDS) and absorption

measurements of control experiments without Rb confirmed the presence of Rb^+ in the NPs.

Results and discussion

Figure 1 presents calculations of the TFs of several perovskite compositions. In the x-axis, increasing Rb^+ contents ($\text{Rb}^+:\text{Cs}^+$ as the A-cation) are presented according to the formula $\text{Rb}_x\text{Cs}_{1-x}\text{PbX}_3$ (x values=0, 0.2, 0.4, 0.6, 0.8, 1; X=Cl, Br, I). The effective ionic radii were taken from the work of Shannon²⁶, considering the coordination number of the ions. For cubic perovskite, the coordination number of the metal and the halide is 6 and for the cation is 12. Here, we assumed that the structural distortion reduced the symmetry of the structure and the coordination number of the cation as well, from 12 to 8, suggested by other paper.²⁷ Thus, the used effective ionic radii are Cs^+ (1.74 Å), Rb^+ (1.61 Å), Pb^{2+} (1.19 Å), Cl^- (1.81 Å), and Br^- (1.96 Å). More details are found in table S1 in the supporting information (SI). The graph shows a linear relation between the TF and the Rb^+ content and suggests that some compositions are expected to form perovskite structure. As the Rb^+ content is higher, the TF is smaller. The dashed line represents the bottom limit of the perovskite formability range. According to the calculated TFs, perovskite crystal structure can be formed while x equals 0.0-1.0 for Cl and Br, and 0.0-0.6 for I, revealing that Cl- and Br- based perovskites have higher chances to form perovskite with higher Rb^+ content. A recent work by Linaburg et al. was focused on the size of the A-cation in bulk mixed-cation perovskites and how it affects their properties.¹³ This work suggested that Rb^+ -based perovskite crystal structure is unstable at room temperature, leading to lattice deformations that result in another Rb^+ -based phases. It is reasonable to assume that the intrinsic strains inside the lattice in the bulk differ from those in the nano-size. Therefore, it is expected that nano-sized particles would provide a more adaptive nature facing A-cation substitutions.^{19,24} This graph gives a prediction for the probability to form Rb-based perovskite from theoretical point of view, yet it cannot assure the formation of stable perovskite in the nominal ratios, which is also different in the bulk and the nano-scale.

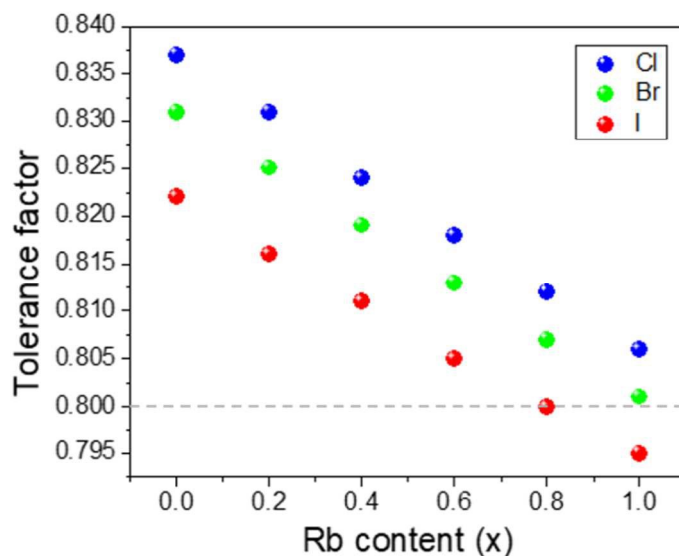


Figure 1. The calculated tolerance factors of $\text{Rb}_x\text{Cs}_{1-x}\text{PbX}_3$ ($X=\text{Cl}, \text{Br}, \text{I}$) perovskites as a function of the Rb content (x), ranges from $x=0$ to $x=1$. The grey dashed line represents the bottom limit of the empirical formability range of perovskite (0.8).

In this work, we successfully demonstrate the possibility to introduce Rb^+ cation with Cs^+ cation in $\text{Rb}_x\text{Cs}_{1-x}\text{PbX}_3$ NPs using hot injection method.¹⁶ Briefly, Rb^+/Cs^+ -oleate precursor was prepared by mixing $\text{Rb}_2\text{CO}_3/\text{Cs}_2\text{CO}_3$ or a mix of them in a 3-neck flask along with oleic acid (OA) and octadecene (ODE). For the lead halide (PbX_2 ; $X=\text{Cl}, \text{Br}$) precursor, PbCl_2 or PbBr_2 were loaded in an additional 3-neck flask along with OA, oleylamine (OLA), and ODE. In the case of PbCl_2 , trioctylphosphine (TOP) was added for a complete dissolution of the salt. Both flasks were degassed under vacuum, and then the temperature was raised to 150 °C for the reaction. A desired volume of Rb^+/Cs^+ -oleate was swiftly injected to the PbX_2 flask. After ~ 5 seconds, an ice bath was applied to quench the reaction. The crude NPs were purified through centrifugation, with isopropanol as an anti-solvent, for further characterizations.

Figure 2 presents the absorption and photoluminescence (PL) spectra of the different mixed-cation perovskite NPs with chloride ($\text{Rb}_x\text{Cs}_{1-x}\text{PbCl}_3$, figure 2a,b) and bromide ($\text{Rb}_x\text{Cs}_{1-x}\text{PbBr}_3$, figure 2c,d). The x values correspond to 0, 0.2, 0.4, 0.6, and 0.8. Clearly, there is a blue shift in absorption and PL towards shorter wavelengths for both chloride and bromide. The NPs with the variable $\text{Rb}^+:\text{Cs}^+$ ratios showed an absorption shift of 0.13 eV and 0.07 eV, respectively. The absorption spectra in figure 2a and 2c confirm that at higher Rb^+ content, the absorption onset shifts to shorter wavelength, while the PL peaks are shifted in the same trend (figure 2b and 2d). The PL derived from the decay of excited mode to the zero- state after excitation, from conduction band to valence band. It should be noted that there is no PL peak for the $x=0.8$ in Cl case due to weak sensitivity of the detector in the spectrofluorimeter in the near UV spectral region. The Mixed cation Rb^+/Cs^+ NPs with iodide as the halide were synthesized and found to be unstable, also showing no optical shift, as shown in figure S1 in the SI. According to the literature, band-gap tuning commonly carried out using mixed-halide systems, however mixed-cation systems are also affecting the band-gap. Many reports about mixed-halide systems and halide-exchange reactions showed a significant optical tuning of perovskite NPs that can be applied to various utilizations.^{16,17,18} Substitutions of the halides influence the electronic and optical properties by changing the energy level of the valence band as a result of different energies of their p orbitals, thus modifying the band-gap.^{28,29} Substitution of the A-cation influences the band-gap indirectly, through structural distortions. As the A-cation size decreases, the Pb-X-Pb angle is more distorted (whether it is larger or smaller than the ideal 180° angle) and the octahedral tilting is larger. This implies that the overlap of the anti-bonding orbitals of the Pb^{2+} metal cation and the halide anion is deformed compared to the ideal cubic perovskite structure. The energies of the valence band and the conduction band are shifting upward, the anti-bonding interaction is weaker, and therefore the Pb-X bonds become more stable.^{16,30} This explains why the energy level of the valence band shifts downward, overall widening the band-gap and shifting the absorption to shorter wavelengths.

A synthesis of $x=1$ (Rb^+ alone as the A-cation) was also implemented with Cl and Br. Cl-based NPs resulted in another phase of $\text{Rb}_6\text{Pb}_5\text{Cl}_{16}$, which presented a remarkable blue shift towards onset of ~ 305 nm (figure S2 in the SI) as reported earlier.²⁵ In the Br case

no NPs were formed. Presumably, perovskite phase was unstable in these conditions. Previous papers report that RbPbX_3 phase can be stabilized only at elevated temperatures (above 320 °C), which explain the results.³¹⁻³⁵

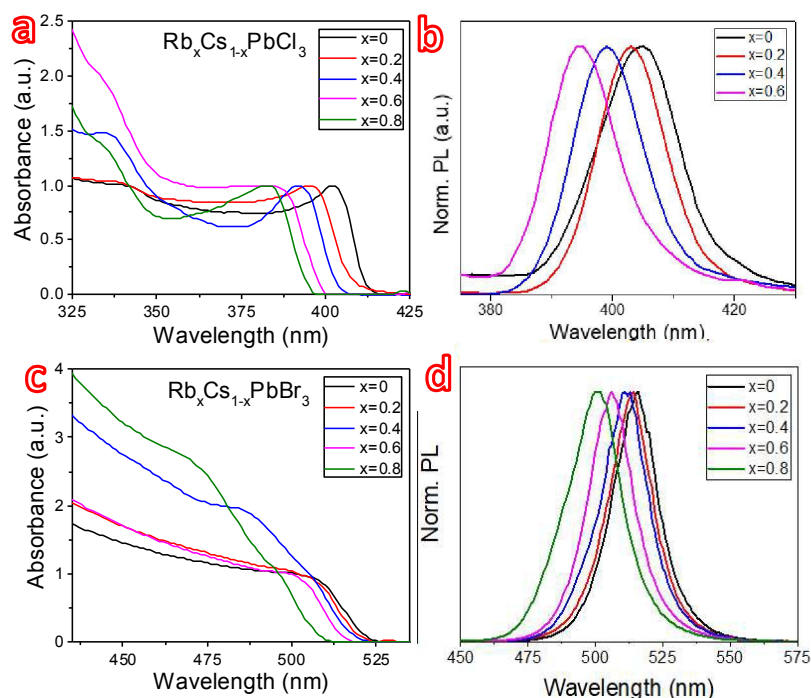


Figure 2. (a,b) Absorbance and normalized photoluminescence (PL) spectra of $\text{Rb}_x\text{Cs}_{1-x}\text{PbCl}_3$ NPs ($x=0, 0.2, 0.4, 0.6, 0.8$). (c,d) Absorbance and normalized PL spectra of $\text{Rb}_x\text{Cs}_{1-x}\text{PbBr}_3$ NPs ($x=0, 0.2, 0.4, 0.6, 0.8$).

Figure 3a shows that the NCs exhibit relatively high PLQYs, which are similar to the ones reported for CsPbX_3 ($X=\text{Cl}, \text{Br}$) NCs. It is hard to distinguish whether there is a pronounced trend while increasing the ratio of $\text{Rb}^+:\text{Cs}^+$. Moreover, the PLQY strongly depends on the purification process of the NPs and the conditions of each synthesis. Moreover, these results suggest that addition of Rb^+ maintains the good PLQY of the CsPbBr_3 NPs.

Figure 3b demonstrates the bright PL of the obtained Br-based NPs under UV light, showing green and turquoise-blue emissions for low and high Rb^+ contents, respectively. The changes in the $\text{Rb}^+:\text{Cs}^+$ ratio is small, therefore only extreme ratios are presented in this picture. The emission of the Cl-based NPs is in the near UV spectral range, so the

change in the emission colors of the NPs with different Rb^+ contents is indistinguishable by human eyes. The influence of adding Rb^+ to Cs-based perovskite NPs is unequivocal in this picture, visualizing the optical measurements (figure 2).

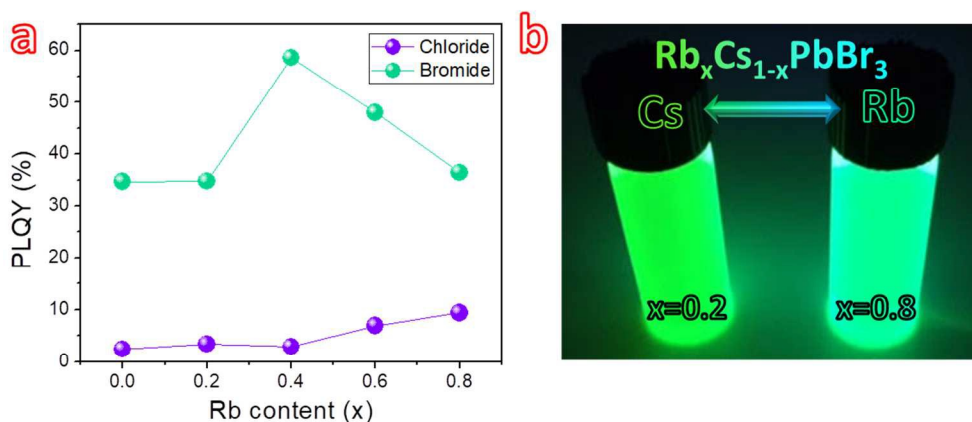


Figure 3. (a) Photoluminescence quantum yield (PLQY) of the NPs with Cl (purple) and Br (green). (b) Photographs of dispersions of $x=0.2$ and $x=0.8$ (left and right vials respectively) samples under ultra-violet light ($\lambda=365$ nm) showing the fluorescence for the extreme molar ratios of Br-based NPs.

The crystal structures of $\text{Rb}_x\text{Cs}_{1-x}\text{PbX}_3$ ($x=0, 0.2, 0.4, 0.6, 0.8, 1$; $X=\text{Cl}, \text{Br}$) NPs were measured by powder x-ray diffraction (PXRD) and the results are presented in figure 4. The diffractograms show that in both cases, a perovskite crystal structure was detected for low Rb^+ contents. In figure 4a, $x=0$ is characterized with peaks that correspond to an orthorhombic CsPbCl_3 perovskite structure. A cubic structure also fitted to the observed peaks, however, it was previously reported that CsPbCl_3 has an orthorhombic symmetry.¹³ Higher Rb^+ contents of $x=0.2$ and $x=0.4$ resulted in the same CsPbCl_3 perovskite peaks. The observed slight shift of the perovskite peaks is associated with small changes of the values of the unit cell parameters upon Rb-Cs substitution. When increasing the Rb^+ content further, the set of perovskite peaks became weaker, and additional peaks had emerged. For example, at $x=0.6$ and $x=0.8$ peaks of RbPb_2Cl_5 phase were detected (see Fig.S2c) while at $x=0.8$ peaks of orthorhombic perovskite are absent. Finally, the product of $x=1$ presented a different set of peaks, which correspond to a tetragonal $\text{Rb}_6\text{Pb}_5\text{Cl}_{16}$ phase rather than perovskite RbPbCl_3 , as mentioned earlier.

A synthesis of $\text{Rb}_6\text{Pb}_5\text{Cl}_{16}$ NPs was recently published by us.²⁵ These observations indicate a change in the crystal structure triggered by replacing the Cs^+ cation with the smaller Rb^+ cation in the lattice, supporting the optical measurements that indicated mixed Rb^+/Cs^+ perovskite NPs. It can be assumed that increasing further the Rb^+ content, at the expense of Cs^+ , disrupts the perovskite stabilization due to geometrical considerations of the cations radii. More details about the detected phases in each ratio are given in Table S2 (SI section).

In figure 4b, the obtained peaks for $x=0$ correspond to an orthorhombic CsPbBr_3 perovskite structure. Low Rb^+ contents yielded in the same perovskite crystal structure, excluding the $x=0.2$ case, in which two intense peaks are observed. These peaks may relate to impurities of Cs_4PbBr_6 phase that is characterized by peaks in the angles 12.8 and 25.9 that can correspond to the observed peaks. In $x=0.6$ and $x=0.8$ cases, peaks of Rb_4PbBr_6 and RbPb_2Br_5 phases were observed (see table S2 for more details). According to the literature, the Rb_4PbBr_6 phase was previously obtained using solid state reactions, starting from binary precursors.³⁶ The possibility for a presence of a small impurity of additional phases ($\text{Rb}_6\text{Pb}_5\text{Cl}_{16}$, RbPb_2Cl_5 , Rb_2PbCl_4 , Rb_3PbCl_5 , RbPb_2Br_5) in the synthesized material is noted by other reports also. From the phase diagram reported by Monzel et al.³⁵ a 1:1 mixture (i.e. RbPbCl_3) will not form a single perovskite phase at room temperature but instead it will form a two-phase mixture. In this work, this phase was proved to crystallize in a rhombohedral K_4CdCl_6 -type structure in contrast to an earlier paper, which suggested a tetragonal Tl_4HgBr_6 -type structure.³⁷ Minimizing the structure to the nano-scale, here the PXRD results stated a tetragonal Rb_4PbBr_6 structure in $x=0.6$ and $x=0.8$ products. The reasons to declare one phase over the other are stability-related. It was concluded that only ns^2 -type of A-cations (such as In^+ and Tl^+) can stabilize the tetragonal Tl_4HgBr_6 -type structure due to polarizations effects and high electronegativity, compared with alkali ions of comparable size, such as Rb^+ . Possibly, a much “looser” crystal structure is forming in the nano-scale, which contributes to the formability of less-preferred structure type.³⁸

More concisely, there is a gradual process of phase modifications in both Cl- and Br-based NPs with increasing the amount of Rb^+ (over Cs). It happens due to the octahedral tilting, when the octahedral tilting is large, a more stable crystal phase is formed until the

perovskite crystal structure is lost completely (for example in Cl; where $x=1$). In the case of Br-based NPs, the NPs formation was restricted to a maximal ratio of $x=0.8$, unable to form a stable perovskite structure with Rb^+ alone.

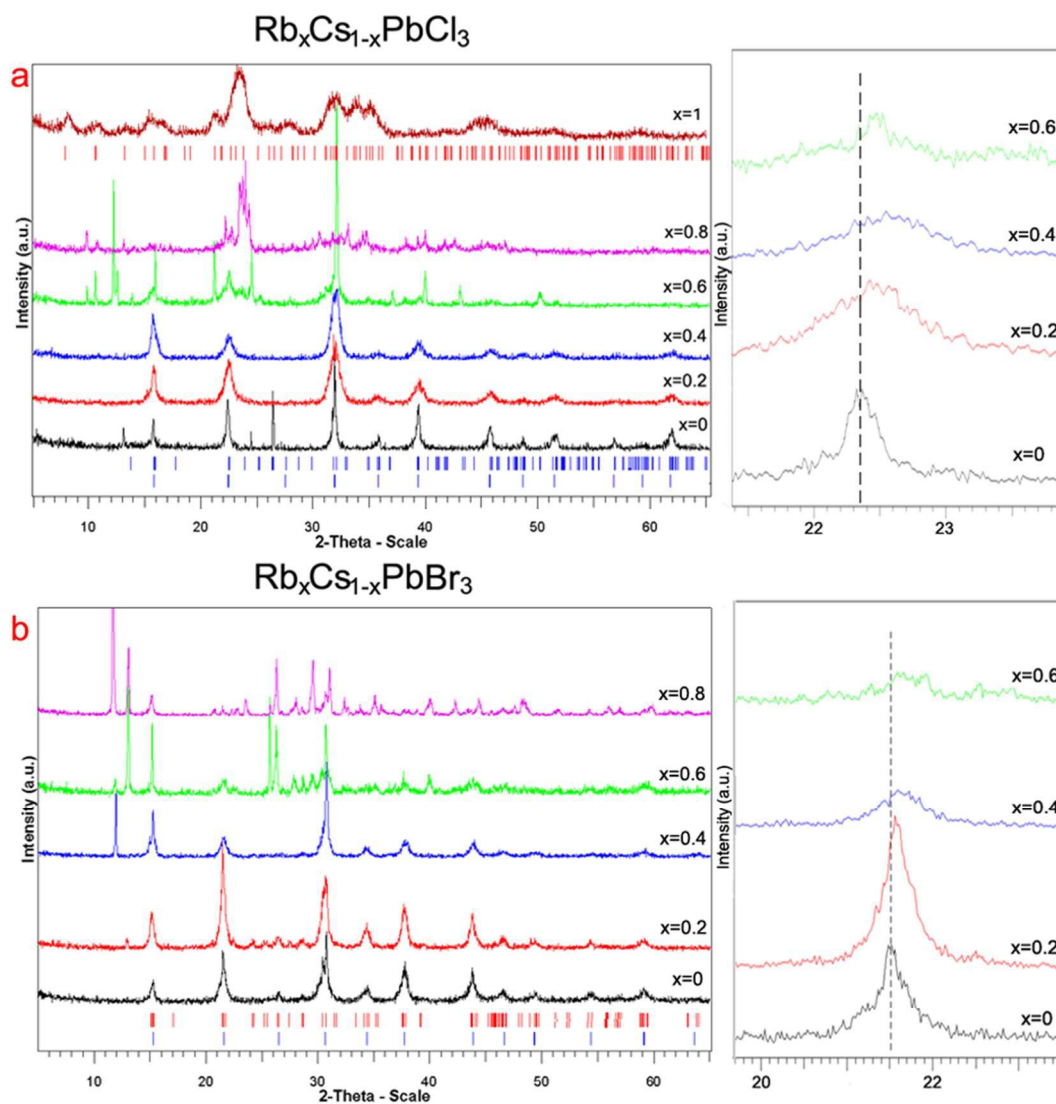


Figure 4. Powder x-ray diffraction (PXRD) patterns for $\text{Rb}_x\text{Cs}_{1-x}\text{PbCl}_3$ ($x=0$ to $x=1$) NPs. (b) PXRD patterns for $\text{Rb}_x\text{Cs}_{1-x}\text{PbBr}_3$ ($x=0$ to $x=0.8$) NPs. Theoretical peak positions of orthorhombic and cubic (for comparison) CsPbCl_3 (a), CsPbBr_3 (b) and tetragonal $\text{Rb}_6\text{Pb}_3\text{Cl}_{16}$ phase (top of (a)) are shown by vertical bars, on the right are zoomed fragments of XRD patterns

Figure 5 depicts transmission electron microscope (TEM) images of the different NPs with a squared shape. Size distributions of each product, with different Rb^+ content, were measured using ImageJ software (figure S3 in the SI). Accordingly, figure S3 presents

the size distributions and the average side length of the NCs, assuming a squared shape. The size distributions along with the average side lengths of the NPs show a declining trend with the increase of Rb^+ content for both Cl and Br. When adding more rubidium to the crystal, at the expense of cesium, the d-spacing among the crystallographic planes is decreasing because Rb^+ is smaller than Cs^+ , affecting the average size of the NPs. One can wonder if the optical blue shifts of the NPs with increasing Rb^+ amounts originate from quantum confinement rather than octahedral tilting. It was suggested that the influence of substituting the monovalent cation depends on the crystalline symmetry of the system.³⁹ If the starting perovskite phase is cubic, replacing the original cation results in a change in the lattice parameters, therefore expansion or contraction of the lattice. If the starting system is tetragonal or orthorhombic, A-cation substitution produces two competing effects regarding both the crystal size and tilting angles of the octahedra. On the one hand, smaller A-cation can cause the lattice to shrink, thus strengthen the antibonding overlap between X-*p* and Pb-*s* orbitals. On the other hand, small A-cation increase the Pb-X-Pb angle, thus weakens the *p-s* overlap. Simulations by Meloni et al. determined that typically the second effect dominates, overall lowering the conduction band and increasing the band-gap.³⁹ We conclude that both affects occur, but the contraction of the lattice upon Rb^+ addition will not cause quantum confinement because the average size is above the Bohr diameter of the NPs, which is 5 nm and 7 nm for CsPbCl_3 and CsPbBr_3 respectively.¹⁹ Therefore, the optical change is associated with the octahedral tilting.

Furthermore, a control experiment was performed in order to ensure that the addition of Rb^+ causes the changes in the optical properties. $\text{Cs}_{0.2}\text{PbBr}_3$, $\text{Cs}_{0.4}\text{PbBr}_3$ and $\text{Cs}_{0.8}\text{PbBr}_3$ without Rb^+ were synthesized (importantly, these chemical formulas indicate the composition at the preparation of the solution, which emphasize that no Rb^+ was used), their absorption spectra were compared to the corresponding absorption of the syntheses with Rb^+ (i.e. $\text{Cs}_{0.2}\text{Rb}_{0.8}\text{PbBr}_3$, $\text{Cs}_{0.4}\text{Rb}_{0.6}\text{PbBr}_3$ and $\text{Cs}_{0.8}\text{Rb}_{0.2}\text{PbBr}_3$ as shown in figure 6). It can be seen from figure 6d that changing the Cs concentration results in a shift of the absorption, however figures 6a, 6b and 6c show that when Rb^+ is added to the NPs the absorption spectra are further blue shifted than without Rb^+ . This provide an additional confirmation that the optical changes are a result of the presence of Rb in the NPs. An

XRD measurement of $\text{Cs}_{0.2}\text{PbBr}_3$ also shows that perovskite in the orthorhombic phase is formed in this case although a reduced amount of Cs is used in the synthesis (see figure S7 in SI). It can be concluded that the amount of Cs in the synthesis affects mainly the amount of the NPs which are formed.

Apart from the size, also the shape is getting less defined with higher Rb^+ contents. It can be related to the change in the crystal phase that may occur due to serious deformations of the perovskite phase into a mix of Cs^+ and Rb^+ -based phases, as the PXRD confirms.

Moreover, black dots appear in all the images. A recent work investigated this issue thoroughly and showed that the black dots are Pb^0 seeds that nucleate prior the reaction in the PbX_2 flask. According to these findings, the use of Rb^+ in the same molar ratio as its Cs^+ counterpart is probably insufficient for a complete crystallization, thus more Pb^0 seeds appear at higher Rb^+ concentrations.⁴⁰

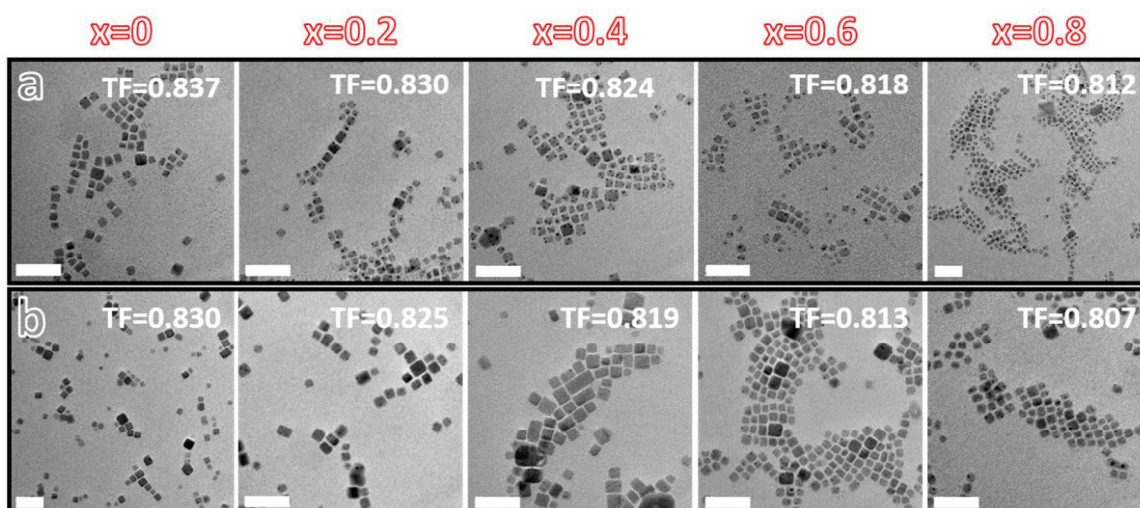


Figure 5. (a) Transmission electron microscope (TEM) images of $\text{Rb}_x\text{Cs}_{1-x}\text{PbCl}_3$ ($x=0, 0.2, 0.4, 0.6, 0.8$) NPs with the corresponding tolerance factors (TF). (b) TEM images of $\text{Rb}_x\text{Cs}_{1-x}\text{PbBr}_3$ ($x=0, 0.2, 0.4, 0.6, 0.8$) NPs with the corresponding TF. The scale bars correspond to 50 nm.

Energy dispersive x-ray spectroscopy (EDS) were used to get an estimation of the elemental composition of the NPs. These measures were collected in scanning transmission electron microscopy (STEM) mode. EDS quantification data for $x=0.8$, for both Cl and Br products, are found in figures S4, S5 and confirm that the NPs are composed of Rb, Cs, Pb, and Cl/Br. In the case of $\text{Rb}_{0.8}\text{Cs}_{0.2}\text{PbCl}_3$, the atomic ratios are 19.14 (Rb), 12.83 (Cs), 38.98 (Pb), and 29.04 (Cl). The atomic ratio between Rb and Cs do not agree with the expectation of 1:4 based on the molar ratio, yet there is more Rb

than Cs in the examined NPs. The ratio between Rb/Cs (as the A-cation) and Pb is 1.2, which is close to the expected ratio (1:1). The atomic percentage of Cl is deviated from the anticipated content, which supposed to be three times larger than Rb/Cs or Pb according to ABX_3 formula. However, Cs-based inorganic perovskite NPs are known to quickly degrade during TEM and STEM analysis because of the electron beam. In the case of Br, the atomic percentage of Rb/Cs together is lower than expected and differs from the Cl-based NPs. Unexpectedly, the Cs content is higher than the Rb content. In addition, the atomic contents of Br and Pb are 60.39% and 23.98% respectively, which meet the expectations. We can predict the following; 1) Cl evaporated as Cl_2 during the measurement and this can result in de-stabilization of the perovskite structure. Therefore, Pb^{2+} cations can undergo reduction by the energized electrons of the beam. 2) In Br-based perovskite NPs, the Rb^+ is less affecting the crystal. This conclusion agrees with the milder change in absorption while adding more Rb^+ , in contrast to Cl-based perovskite NPs. It is also supported by the calculated TF (figure 1) for Br-based perovskite NPs, which is less stable when increasing the Rb^+ content compared with Cl-based perovskite NPs. It is important to note that the nominal ratios between Cs^+ and Rb^+ are theoretical and are limited in predicting the real ratios in the as-synthesized NPs. The stability of the NPs was measured by tracking the absorption of the NPs once a week for a whole month. All NPs showed a red shift in absorption on the first week after the synthesis. No more changes in the absorption were observed afterwards (figure S6). The chloride NPs were less stable as the absorption spectra of the different concentrations were merged together after the first week while the bromide based NPs keep the difference in the absorption spectra for the whole month.

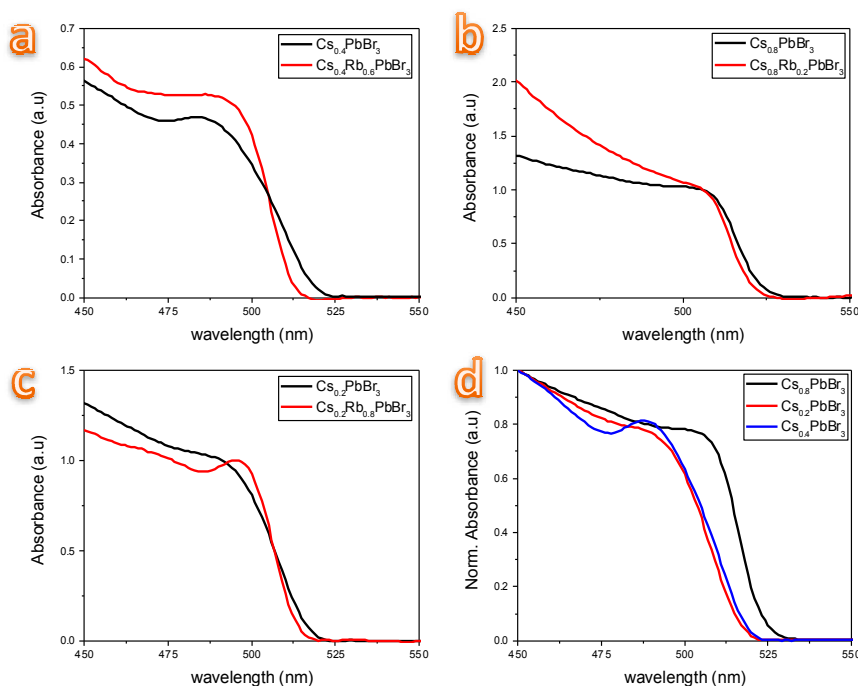


Figure 6. (a) Absorbance of $\text{Cs}_{0.2}\text{PbBr}_3$ and $\text{Cs}_{0.2}\text{Rb}_{0.8}\text{PbBr}_3$. (b) Absorbance of $\text{Cs}_{0.4}\text{PbBr}_3$ and $\text{Cs}_{0.4}\text{Rb}_{0.6}\text{PbBr}_3$. (c) Absorbance of $\text{Cs}_{0.2}\text{PbBr}_3$ and $\text{Cs}_{0.2}\text{Rb}_{0.8}\text{PbBr}_3$. (d) Absorbance of $\text{Cs}_{0.2}\text{PbBr}_3$, $\text{Cs}_{0.4}\text{PbBr}_3$ and $\text{Cs}_{0.8}\text{PbBr}_3$.

Experimental

Chemicals. Cesium carbonate (Cs_2CO_3 , 99.9%, Sigma-Aldrich), rubidium carbonate (Rb_2CO_3 , 99%, Sigma-Aldrich), lead (II) chloride (PbCl_2 , 98%, Sigma-Aldrich), lead (II) bromide (PbBr_2 , $\geq 98\%$, Sigma-Aldrich), oleic acid (OA, 90%, Sigma-Aldrich), oleylamine (OLAM, 70%, Sigma-Aldrich), trioctylphosphine (TOP, 97%, Strem), 1-octadecene (ODE, 90%, Sigma-Aldrich), 2-propanol ($\geq 99.8\%$, Sigma-Aldrich), and hexane (not pure, Gadot) were purchased and used as received, without any further purification.

Preparation of Rb/Cs-oleate. Rb/Cs-oleate precursor was prepared according to previous published procedure by Protesescue et al.¹⁶ Different molar ratios of $\text{Cs}_2\text{CO}_3/\text{Rb}_2\text{CO}_3$ (total of 1.228 mmol) were mixed with 625 μL of oleic acid (OA) and 7.5 mL of 1-octadecene (ODE) in a 50 mL 3-neck flask. The solution was degassed for 1h under vacuum conditions at 120 $^\circ\text{C}$ and then heated to 150 $^\circ\text{C}$ under Ar flow.

Synthesis of $\text{Rb}_x\text{Cs}_{1-x}\text{PbX}_3$ (X=Cl, Br) NPs. The NPs were synthesized according to Protesescue et al.. 0.188 mmol of PbX_2 were mixed with 0.5 mL of OA, 0.5 mL of OLA, and 5 mL of ODE in an additional 100 mL 3-neck flask. 1 mL of TOP was added in the case of PbCl_2 . The solution was degassed for 1h under vacuum at 120 °C and then heated to 150 °C under Argon flow. The reaction was carried out by injection of 0.4 mL of the Rb/Cs-oleate precursor solution into the PbX_2 precursor solution using a preheated syringe. The reaction was quenched using an ice bath after a few seconds. The crude solution was centrifuged at 8000 rpm for 10 min. Isopropanol was added in a volume ratio of 1:1 and the NCs were centrifuged again at 6000 rpm for 10 min. The purified NCs were dispersed in hexane for further characterization.

High resolution Transmission Electron Microscopy (HRTEM). Morphology and elemental composition of the NPs were analyzed with HR (S)TEM (High Resolution Scanning Transmission Electron Microscope) Tecnai F20 G2 (FEI Company, U.S.A.). Samples preparation was performed as follows: 3.5 μL of the NCs dispersion were dropped on a copper grid coated with amorphous carbon film, and then the solvent was evaporated using a vacuum chamber. Elemental analysis of NCs was done with EDAX EDS (Energy Dispersive X-Ray Spectroscopy) when the microscope was operated in STEM mode at accelerating voltage 200 kV.

Powder X-ray Diffraction (PXRD). Powder X-ray diffraction measurements were performed in grazing incidence X-ray diffraction (GIXRD) mode on the D8 Advance Diffractometer (Bruker AXS, Karlsruhe, Germany) with a goniometer radius of 217.5 mm, a secondary graphite monochromator, 2° Soller slits, and a 0.2 mm receiving slit. XRD patterns within the range 3–60° 2 θ were recorded at room temperature using CuK α radiation (1 1/ 4 1.5418°A) with the following measurement conditions: tube voltage of 40 kV, tube current of 40 mA, step-scan mode with a step size of 0.02° 2 θ , and counting time of 1–3 s per step. The value of the grazing incidence angle was 2.5°.

Optical measurements. Absorption spectra were recorded using Jasco V- 670 spectrophotometer. Photoluminescence (PL) measurements were performed using L-shaped spectrofluorometer (Edinburgh Instruments FL920). The Cl- and Br-based NPs were excited at 320 and 400 nm respectively. The emission was collected at 90° at the

range of 350–440 nm for Cl and 450–550 nm for Br. Photoluminescence quantum yields (PLQY) were measured using Hamamatsu absolute PLQY spectrometer C11347.

Conclusions

This paper describes the introduction of Rb^+ cation into CsPbX_3 NPs. The addition of small Rb^+ cation in increasing ratios affects the levels of structural pressure on the inorganic CsPbX_3 ($X=\text{Cl}, \text{Br}$) perovskite NPs. $\text{Rb}_x\text{Cs}_{1-x}\text{PbX}_3$ ($X=\text{Cl}, \text{Br}$) systems were recently reported for solid solutions and found to have tunable optical properties. This was explained by an increase of octahedral tilting, which affects the anti-bonding overlap of the Pb^{2+} and the X^- orbitals.¹³ However, in this paper the synthesis and characterization of $\text{Rb}_x\text{Cs}_{1-x}\text{PbX}_3$ NPs were developed to have more comprehensive knowledge about the structural and optical consequences of A-cation modifications in the nano-scale, which opens a window for high structural flexibility. The obtained NPs were characterized and found to exhibit high PLQYs, which are comparable to those of the original CsPbX_3 nanoparticles. In addition, the band-gaps of Cl- and Br-based NPs could be enlarged by increasing the amount of Rb^+ in the crystal. TEM images showed square-shaped NPs and EDS elemental analysis confirmed the presence of Rb^+ in the NPs. Although calculations of the tolerance factors of these NPs predicted that high contents of Rb^+ yield are close to the lower limit of the perovskite formability range that can lead to unstable perovskites, the results proved that mixed-cation perovskite NPs are indeed formed, possessing properties that are very similar to the known CsPbX_3 NPs. The possibility to obtain a mild band-gap tuning for Rb^+/Cs^+ mixed-cation NPs is one step forward to full understanding of perovskite nanostructures. Future experiments can be attributed to apply these NPs for light emitting devices or as thin films that may enhance the performance of perovskite solar cells.

Supporting Information

The supporting information includes: Absorption, XRD analysis and EDS elemental analysis.

Acknowledgments

This work was supported by the Israel ministry of energy and the Israel ministry of the chief scientist.

References

- ¹ Stoumpos, Constantinos C., Christos D. Malliakas, and Mercouri G. Kanatzidis. "Semiconducting tin and lead iodide perovskites with organic cations: phase transitions, high mobilities, and near-infrared photoluminescent properties." *Inorganic chemistry* 52, no. 15 (2013): 9019-9038.
- ² Noh, Jun Hong, Sang Hyuk Im, Jin Hyuck Heo, Tarak N. Mandal, and Sang Il Seok. "Chemical management for colorful, efficient, and stable inorganic–organic hybrid nanostructured solar cells." *Nano letters* 13, no. 4 (2013): 1764-1769.
- ³ Hao, Feng, Constantinos C. Stoumpos, Robert PH Chang, and Mercouri G. Kanatzidis. "Anomalous band gap behavior in mixed Sn and Pb perovskites enables broadening of absorption spectrum in solar cells." *Journal of the American Chemical Society* 136, no. 22 (2014): 8094-8099.
- ⁴ Filip, Marina R., Giles E. Eperon, Henry J. Snaith, and Feliciano Giustino. "Steric engineering of metal-halide perovskites with tunable optical band gaps." *Nature communications* 5, no. 5757 (2014): 1-9.
- ⁵ Amat, Anna, Edoardo Mosconi, Enrico Ronca, Claudio Quarti, Paolo Umari, Md K. Nazeeruddin, Michael Grätzel, and Filippo De Angelis. "Cation-induced band-gap tuning in organohalide perovskites: interplay of spin–orbit coupling and octahedra tilting." *Nano letters* 14, no. 6 (2014): 3608-3616.
- ⁶ Stoumpos, Constantinos C., Laszlo Frazer, Daniel J. Clark, Yong Soo Kim, Sonny H. Rhim, Arthur J. Freeman, John B. Ketterson, Joon I. Jang, and Mercouri G. Kanatzidis. "Hybrid germanium iodide perovskite semiconductors: active lone pairs, structural distortions, direct and indirect energy gaps, and strong nonlinear optical properties." *J. Am. Chem. Soc* 137, no. 21 (2015): 6804-6819.
- ⁷ Liu, Wenyong, Qianglu Lin, Hongbo Li, Kaifeng Wu, István Robel, Jeffrey M. Pietryga, and Victor I. Klimov. "Mn²⁺-Doped lead halide perovskite nanocrystals with

dual-color emission controlled by halide content." *J. Am. Chem. Soc.* 138, no. 45 (2016): 14954-14961.

⁸ Parobek, David, Benjamin J. Roman, Yitong Dong, Ho Jin, Elbert Lee, Matthew Sheldon, and Dong Hee Son. "Exciton-to-dopant energy transfer in Mn-doped cesium lead halide perovskite nanocrystals." *Nano Lett* 16, no. 12 (2016): 7376-7380.

⁹ Liu, Huiwen, Zhennan Wu, Jieren Shao, Dong Yao, Hang Gao, Yi Liu, Weili Yu, Hao Zhang, and Bai Yang. "CsPb_xMn_{1-x}Cl₃ Perovskite Quantum Dots with High Mn Substitution Ratio." *ACS nano* 11, no. 2 (2017): 2239-2247.

¹⁰ Duong, The, Hemant Kumar Mulmudi, Heping Shen, YiLiang Wu, Chog Barugkin, Yahuitl Osorio Mayon, Hieu T. Nguyen et al. "Structural engineering using rubidium iodide as a dopant under excess lead iodide conditions for high efficiency and stable perovskites." *Nano Energy* 30 (2016): 330-340.

¹¹ Duong, The, YiLiang Wu, Heping Shen, Jun Peng, Xiao Fu, Daniel Jacobs, Er-Chien Wang et al. "Rubidium Multication Perovskite with Optimized Bandgap for Perovskite-Silicon Tandem with over 26% Efficiency." *Advanced Energy Materials* (2017).

¹² Saliba, Michael, Taisuke Matsui, Konrad Domanski, Ji-Youn Seo, Amita Ummadisingu, Shaik M. Zakeeruddin, Juan-Pablo Correa-Baena et al. "Incorporation of rubidium cations into perovskite solar cells improves photovoltaic performance." *Science* 354, 6309 (2016): 206-209.

¹³ Linaburg, Matthew R., Eric T. McClure, Jackson D. Majher, and Patrick M. Woodward. "Cs_{1-x}Rb_xPbCl₃ and Cs_{1-x}Rb_xPbBr₃ Solid Solutions: Understanding Octahedral Tilting in Lead Halide Perovskites." *Chemistry of Materials* 29, no. 8 (2017): 3507-3514.

¹⁴ <https://www.nrel.gov/pv/assets/images/efficiency-chart.png> (24.12.17)

¹⁵ Yang, Woon Seok, Byung-Wook Park, Eui Hyuk Jung, Nam Joong Jeon, Young Chan Kim, Dong Uk Lee, Seong Sik Shin et al. "Iodide management in formamidinium-lead-halide-based perovskite layers for efficient solar cells." *Science* 356, no. 6345 (2017): 1376-1379.

¹⁶ Protesescu, Loredana, Sergii Yakunin, Maryna I. Bodnarchuk, Franziska Krieg, Riccarda Caputo, Christopher H. Hendon, Ruo Xi Yang, Aron Walsh, and Maksym V.

Kovalenko. "Nanocrystals of cesium lead halide perovskites (CsPbX₃, X= Cl, Br, and I): novel optoelectronic materials showing bright emission with wide color gamut." *Nano Lett* 15, no. 6 (2015): 3692-3696.

¹⁷ Nedelcu, Georgian, Loredana Protesescu, Sergii Yakunin, Maryna I. Bodnarchuk, Matthias J. Grotevent, and Maksym V. Kovalenko. "Fast anion-exchange in highly luminescent nanocrystals of cesium lead halide perovskites (CsPbX₃, X= Cl, Br, I)." *Nano Letters* 15, no. 8 (2015): 5635-5640.

¹⁸ Akkerman, Quinten A., Valerio D'Innocenzo, Sara Accornero, Alice Scarpellini, Annamaria Petrozza, Mirko Prato, and Liberato Manna. "Tuning the optical properties of cesium lead halide perovskite nanocrystals by anion exchange reactions." *Journal of the American Chemical Society* 137, no. 32 (2015): 10276-10281.

¹⁹ Protesescu, Loredana, Sergii Yakunin, Sudhir Kumar, Janine Bär, Federica Bertolotti, Norberto Masciocchi, Antonietta Guagliardi et al. "Dismantling the "Red Wall" of Colloidal Perovskites: Highly Luminescent Formamidinium and Formamidinium–Cesium Lead Iodide Nanocrystals." *Acs Nano* 11, no. 3 (2017): 3119-3134.

²⁰ Goldschmidt, Victor Moritz. "Die gesetze der krystallochemie." *Naturwissenschaften* 14, no. 21 (1926): 477-485.

²¹ Kieslich, Gregor, Shijing Sun, and Anthony K. Cheetham. "An extended tolerance factor approach for organic–inorganic perovskites." *Chemical Science* 6, no. 6 (2015): 3430-3433.

²² Travis, W., E. N. K. Glover, H. Bronstein, D. O. Scanlon, and R. G. Palgrave. "On the application of the tolerance factor to inorganic and hybrid halide perovskites: a revised system." *Chemical Science* 7, no. 7 (2016): 4548-4556.

²³ Green, Martin A., Anita Ho-Baillie, and Henry J. Snaith. "The emergence of perovskite solar cells." *Nature Photonics* 8, no. 7 (2014): 506-514.

²⁴ Huang, He, Maryna Bodnarchuk, Stephen V. Kershaw, Maksym V. Kovalenko, and Andrey L. Rogach. "Lead Halide Perovskite Nanocrystals in the Research Spotlight: Stability and Defect-Tolerance." *ACS Energy Letters* 2, (2017):2071-2083.

- ²⁵ Amgar, Daniel, Malgorzata Wierzbowska, Vladimir Uvarov, Vitaly Gutkin, and Lioz Etgar. "Novel rubidium lead chloride nanocrystals: synthesis and characterization." *Nano Futures* (2017), 1: 021002.
- ²⁶ Shannon, Robert D. "Revised effective ionic radii and systematic studies of interatomic distances in halides and chalcogenides." *Acta crystallographica section A: crystal physics, diffraction, theoretical and general crystallography* 32, no. 5 (1976): 751-767.
- ²⁷ Mitchell, Roger H., Mark D. Welch, and Anton R. Chakhmouradian. "Nomenclature of the perovskite supergroup: A hierarchical system of classification based on crystal structure and composition." *Mineralogical Magazine* 81, no. 3 (2017): 411-461.
- ²⁸ Chang, Y. H., C. H. Park, and K. Matsuishi. "First-Principles Study of the Structural and the Electronic Properties of the Lead-Halide-Based Inorganic-Organic Perovskites (CH₃NH₃)PbX₃ and CsPbX₃ (X= Cl, Br, I)." *Journal-Korean Physical Society* 44 (2004): 889-893.
- ²⁹ Butler, Keith T., Jarvist M. Frost, and Aron Walsh. "Band alignment of the hybrid halide perovskites CH₃NH₃PbCl₃, CH₃NH₃PbBr₃ and CH₃NH₃PbI₃." *Materials Horizons* 2, no. 2 (2015): 228-231.
- ³⁰ Eperon, Giles E., Samuel D. Stranks, Christopher Menelaou, Michael B. Johnston, Laura M. Herz, and Henry J. Snaith. "Formamidinium lead trihalide: a broadly tunable perovskite for efficient planar heterojunction solar cells." *Energy & Environmental Science* 7, no. 3 (2014): 982-988.
- ³¹ K. Treis, *Neues Jahrbuch Mineral. Geol.* 1914, 37, 784.
- ³² Glazer, A. M. "The classification of tilted octahedra in perovskites." *Acta Crystallographica Section B: Structural Crystallography and Crystal Chemistry* 28, no. 11 (1972): 3384-3392.
- ³³ Beck, Horst P., Manfred Schramm, Robert Haberkorn, Robert Dinnebier, and Peter W. Stephens. "Synthesis and Crystal Structure of Rb₆Pb₅Cl₁₆." *Zeitschrift für Anorganische und Allgemeine Chemie* 624 (1998): 393-398.
- ³⁴ Howard, Christopher J., and Harold T. Stokes. "Group-theoretical analysis of octahedral tilting in perovskites." *Acta Crystallographica Section B: Structural Science* 54, no. 6 (1998): 782-789.

- ³⁵ Monzel, H., M. Schramm, K. StoÈwe, and H. P. Beck. "Zur Neuuntersuchung des Phasendiagramms RbCl/PbCl₂." *Zeitschrift für anorganische und allgemeine Chemie* 626, no. 2 (2000): 408-411.
- ³⁶ Beck, H. P., and W. Milius. "Study on A₄BX₆ Compounds. II [1]. Refinement of the Structure of Rb₄PbBr₆ and a Note on the Existence of "Rb₄Hgl₆" and "K₄CdI₆." *Zeitschrift für anorganische und allgemeine Chemie* 562, no. 1 (1988): 102-104.
- ³⁷ Cola, Mario, Vincenzo Massarotti, Riccardo Riccardi, and Cesare Sinistri. "Binary systems formed by lead bromide with (Li, Na, K, Rb, Cs and Tl) Br: a DTA and diffractometric study." *Zeitschrift für Naturforschung A* 26, no. 8 (1971): 1328-1332.
- ³⁸ Beck, H. P., and W. Milius. "Study on A₄BX₆ Compounds. III [1]. ns² cations as a prerequisite for a structure type and their interaction in ternary halides with the formula type A₄BX₆ (A: In, Tl; B: Cd, Pb, Ge; X: Cl, Br, I)." *Zeitschrift für anorganische und allgemeine Chemie* 562, no. 1 (1988): 105-114.
- ³⁹ Meloni, Simone, Giulia Palermo, Negar Ashari Astani, Basile FE Curchod, Michael Graetzel, and Ursula Roethlisberger. "Valence and conduction bands engineering in halide perovskites for solar cell applica-tions." *arXiv preprint arXiv:1412.3659* (2014).
- ⁴⁰ Udayabhaskararao, Thumu, Miri Kazes, Lothar Houben, Hong Lin, and Dan Oron. "Nucleation, Growth, and Structural Transformations of Perovskite Nanocrystals." *Chem. Mater* 29, no. 3 (2017): 1302-1308.